

Analysis of motoneuron responses to composite synaptic volleys (computer simulation study)

Maria Piotrkiewicz · Lydia Kudina

Received: 4 August 2011 / Accepted: 9 December 2011 / Published online: 24 December 2011
© The Author(s) 2011. This article is published with open access at Springerlink.com

Abstract This paper deals with the analysis of changes in motoneuron (MN) firing evoked by repetitively applied stimuli aimed toward extracting information about the underlying synaptic volleys. Spike trains were obtained from computer simulations based on a threshold-crossing model of tonically firing MN, subjected to stimulation producing postsynaptic potentials (PSPs) of various parameters. These trains were analyzed as experimental results, using the output measures that were previously shown to be most effective for this purpose: peristimulus time histogram, raster plot and peristimulus time intervalgram. The analysis started from the effects of single excitatory and inhibitory PSPs (EPSPs and IPSPs). The conclusions drawn from this analysis allowed the explanation of the results of more complex synaptic volleys, i.e., combinations of EPSPs and IPSPs, and the formulation of directions for decoding the results of human neurophysiological experiments in which the responses of tonically firing MNs to nerve stimulation are analyzed.

Keywords Human motoneuron · Computer simulation · Postsynaptic potentials · Peristimulus time histogram · Intervalgram and frequencygram · Raster plot

Introduction

During the second half of the last century, an enormous amount of knowledge about mammalian motoneuron (MN) pools was collected. This progress was enabled mostly by the development of the precise techniques of intracellular recordings in acute animal experiments, many of which were conducted under deep anesthesia. Recently, evidence accumulated that an anesthetic may change certain properties of the cell membrane (Guertin and Hounsgaard 1999; Button et al. 2006; Windels and Kiyatkin 2006). Therefore, other solutions are applied, one of which is human experiments, which have recently gained attention also among scientists working with animals (Heckman et al. 2008; Gorassini et al. 2009).

Human experiments have the advantage that here intact MNs are studied in their physiological environment. On the other hand, for obvious reasons, human MN studies rely on indirect measurement methods, so the proper interpretation of their results always requires careful consideration based on the knowledge obtained from animal experiments.

The neuronal circuitry of the human motor control system can be studied experimentally by electrical stimulation of the appropriate nerve during slight muscle contraction and analysis of the stimulus-evoked changes in the MN firing. This approach has been commonly used since the 1970s (e.g. Ashby and Labelle 1977; Kudina 1980, 1988; Awiszus 1988; Miles et al. 1989). Some researchers aimed at estimation of the amplitude and time course of synaptic potentials; however, the interpretations given were often incorrect (for details, see Piotrkiewicz et al. 2009). Usually, during the nerve stimulation, the first to be excited are muscle spindle primary afferents (Ia). In animal experiments, they produce in the MN short excitatory postsynaptic potentials (EPSPs) with durations not exceeding 20 ms and

M. Piotrkiewicz (✉)
Institute of Biocybernetics and Biomedical Engineering,
Polish Academy of Sciences, Warsaw, Poland
e-mail: masia@ibib.waw.pl

L. Kudina
Institute for Information Transmission Problems (Kharkevich
Institute), Russian Academy of Sciences, Moscow, Russia

rise times of 1–2 ms (Coombs et al. 1955; Curtis and Eccles 1959; Burke 1967). Similar time characteristics of Ia EPSPs (5–20 and 2–5 ms, respectively) were estimated in human MNs (Ashby and Zilm 1982a). Yet in later studies, the duration of human Ia EPSPs was claimed to be longer, up to 70 ms (Binboğa et al. 2011).

The important tools for interpreting human data are simulations based on models, both animal (e.g. Türker and Powers 1999, 2002) or computer (e.g. Ashby and Zilm 1982b; Piotrkiewicz et al. 2009). The simulations allow directly comparing the characteristics of various synaptic volleys with the results of their interaction with firing MN revealed by the output measures used for analysis of stimulus-correlated MN firing. We prefer computer simulations, which do not have limitations present in experimental work (e.g. the number of stimuli). In our earlier study (Piotrkiewicz et al. 2009), we performed a detailed analysis of stimulus-evoked changes in MN discharge by a single EPSP. The analysis revealed that these changes consist of a single primary and several secondary effects; one of the latter is still interpreted in certain experimental studies as “long-lasting excitation” (e.g. Binboğa et al. 2011; Prasartwuth et al. 2008). That is why we decided to discuss this problem in this paper in more detail.

The particular case considered in (Piotrkiewicz et al. 2009) is not always observed in experiments. More often, nerve stimulation yields results indicating that the experimental synaptic volley results in more than one postsynaptic potential (PSP) evoked in a MN. The purpose of this paper was therefore to provide the analysis of the results evoked also by more complicated synaptic volleys, which may be helpful in decoding synaptic connections.

Methods

The simulations were based on a threshold-crossing model of a rhythmically firing MN (Piotrkiewicz 1999; Piotrkiewicz et al. 2004, 2009). The model differs from other simple models of this type in that it incorporates the majority of the important features of MN rhythmic firing documented in animal experiments, such as postspike threshold variations or synaptic noise.

Model

The principle of the modeling is presented in Fig. 1. An interspike membrane potential trajectory was obtained by summing the waveform representing afterhyperpolarization (AHP) and the waveform representing tonic synaptic inflow. Whenever the resulting potential trajectory crossed

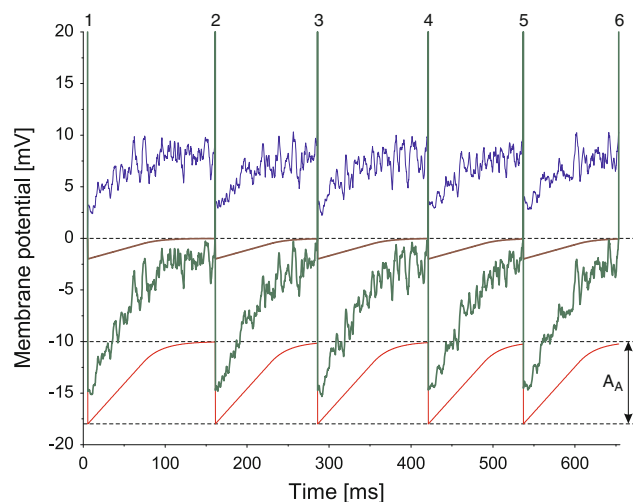


Fig. 1 Principles of the modeling. Traces from bottom to top: AHP curve, interspike membrane potential trajectory, firing threshold time course, tonic synaptic inflow. *Broken lines*: at 0, asymptotic threshold level; at -10 , resting membrane potential A_A , AHP amplitude. Note that all traces are interrupted by spike generation (1, 2, 3, 4, 5, 6) and reset afterward

the firing threshold, the time of MN discharge was recorded, and the whole summation process was reset.

An AHP curve (bottom trace) was described as a combination of a straight line and an exponential:

$$\begin{aligned} V_1(t) &= a \times t + b \quad \text{for } t \leq t_i \\ V_2(t) &= V_0 \exp(-c(t-d)) \quad \text{for } t > t_i, \end{aligned} \quad (1)$$

where t was time (ms), a (mV/ms), slope coefficient (related to AHP duration), b , AHP amplitude A_A (mV), V_0 , a constant of the value -1 mV. Transition time t_i was computed from the voltage level at which straight line and exponential were joined (joint level, JL):

$$t_i = \frac{JL - b}{a} \quad (2)$$

Coefficients c (ms^{-1}) and d (ms) were computed from the condition that the values and derivatives of functions V_1 and V_2 should be equal at the joint level:

$$c = \frac{aV_0}{JL} \quad (3)$$

$$d = t_0 - \frac{\ln(c) - \ln(a)}{c} \quad (4)$$

As seen in Fig. 1, to the AHP trace a constant value of -10 mV was added, which corresponded to the resting potential of the MN.

Tonic synaptic inflow was simulated as a sum of the PSP trains (each train representing the contribution of a single synapse), with inhibitory synaptic potential (IPSP) trains constituting 20% of the total number. A single PSP time course was described by the formula:

$$PSP(t) = Af(\exp(-t/T_1) - \exp(-t/T_2)), \quad (5)$$

where T_2 is a time constant responsible for rising phase, T_1 is a time constant responsible for decaying phase and Af is an amplitude scaling factor. This formula was used in the model for description of both EPSPs (positive Af) and IPSPs (negative Af).

For each EPSP train, EPSP amplitude and mean repetition rate were chosen randomly from the ranges given in Table 1. These parameters were chosen to fit the experimental data on interspike interval (ISI) variability in MNs supplying the brachial biceps (Piotrkiewicz et al. 2001). The consecutive ISIs were computed according to the normal distribution with the mean value equal to the inverse of mean repetition rate and the coefficient of variation equal to 20%.

The amplitude of each PSP (including extra PSPs described below) was multiplied by the coefficient of depression obtained by exponential fit of the experimental data of Coombs et al. (1955, their Fig. 6). The coefficient was equal to 0.3 at the time of spike generation and increased to 0.99 at the time equal AHP duration, so that the PSP amplitude was decreased after the generation of MN action potential and gradually returned to its initial value thereafter. As a result, the inflow level and its variability decreased at the beginning of ISI (Fig. 1, top trace).

The model incorporated the firing threshold changes within the ISI. In accordance with experimental data (Calvin 1974; Powers and Binder 1996), the threshold time course in the model was a scaled down version of the AHP (1). For computational convenience, the asymptotic spike threshold level was set at 0 mV.

Table 1 Model parameters

AHP duration ^a	173.2 ms
AHP amplitude	−8 mV
Potential level, at which triangle and exponential were joined	−2 mV
Threshold amplitude	−2 mV
Parameters of PSP trains (tonic synaptic inflow)	
Rise time	1.2 ms
Half-decay time ^b	4.0 ms
Duration ^c	16.4 ms
Amplitude range	−0.5 to +0.9 mV
Repetition rate range	4–100 s ^{−1}

^a AHP duration was measured from the onset to the time by which it decayed to the value of 0.01 mV below the level of resting membrane potential

^b Measured from the onset of the PSP to the time by which it decayed to the half amplitude

^c Measured from the onset of the PSP to the time by which it decayed to the 0.002 amplitude

The mean firing rate of the model MN could be varied by changing the number of active synapses. The influence of the firing rate on the results was investigated in our previous papers, (Piotrkiewicz et al. 2004) for IPSP and (Piotrkiewicz et al. 2009) for EPSP. In this paper, all the results were obtained for a moderate mean firing rate of about 8 imp/s (corresponding to 186 active synapses).

To simulate the effects of the stimulation, EPSPs and IPSPs in different configurations were added at regular intervals once every 2 s to the resulting membrane potential trajectories. Despite rhythmic stimulation, due to ISI variability, the arrival times of these extra PSPs were randomly distributed with respect to the MN firing. The interstimulus intervals were chosen so that the effects induced by a stimulus disappeared before the delivery of the next stimulus.

The composite synaptic volleys consisted of PSPs with various latencies.

In experiments, each synapse introduces certain jitter with respect to the stimulus timing. The monosynaptic H-reflex has the shortest latency (around 30 ms) and should have the lowest jitter; PSPs arriving with longer latencies are likely to be oligosynaptic, so their jitter values should be considerably higher. Accordingly, each extra PSP was assigned the arbitrarily chosen value of standard deviation of jitter depending on its latency (see Table 2, in which all the parameters of extra PSPs are collected). The jitter was introduced in simulations by modifying the latency for each stimulus and each PSP by a pseudorandom number generated from a normal distribution with a mean value 0 and the respective standard deviation (SD).

Data analysis

The resulting spike trains were used to construct the output measures, as described below. The analysis of motoneuronal responses to the nerve stimulation was performed by means of special software, whose initial version, designed for the analysis of cross-correlations between MN pairs, was described elsewhere (Jakubiec and Piotrkiewicz 2004).

1. Peristimulus time histogram (PSTH, Fig. 2a) presents the number of discharges (ordinate) as a function of peristimulus time, i.e., the time lag between stimulus and discharge time (abscissa). Peristimulus time values may be negative or positive, respectively, for discharges occurring before or after the stimulus. The PSTHs presented here are compiled with 2-ms bins; narrower bins were found to be inappropriate, since they introduced too much variability to the data. The average (solid horizontal line) and SD of count number were determined for background discharges (from the fragment of the PSTH with negative values of peristimulus time). The maximum or minimum was considered significant if the PSTH exceeded significance

Table 2 The parameters of extra PSPs used in the model

Version number	PSP type	Rise time ^a (ms)	Half-decay time ^b (ms)	Duration ^c (ms)	Amplitude (mV)	Latency (ms)	Jitter (SD) [ms]	Figure no.
1	EPSP	3.40	9.80	35.6	2.0	30	0.1	2
2	IPSP	4.00	11.00	38.5	−2.0	34	1.5	3
3	EPSP	1.00	3.00	13.1	1.4	28	0.1	4
	IPSP	4.00	11.00	38.5	−2.0	34	1.5	
4	IPSP	4.00	11.00	38.5	−2.0	28	1.0	5
	EPSP	1.45	4.65	21.4	1.4	41	3.0	
5	EPSP	3.0	8.4	31.6	1.7	41	0.1	7

^a Or duration of hyperpolarizing phase for IPSP

^b Measured from the onset of the PSP to the time by which it decayed to the half amplitude

^c Measured from the onset of the PSP to the time by which it decayed to the 0.002 amplitude

limits, which were calculated as the mean \pm 2.5*SD (dashed horizontal lines).

The strength of the synaptic volley was assessed by the response index (*FI*), calculated as the number of discharges exceeding the mean value for excitation or missing below the mean value for inhibition (shaded areas in Fig. 2a), and normalized to the total number of stimuli (*N*).

$$FI = \frac{\sum_{i=j}^{i=k} (x_i - \bar{x})}{N} \quad (6)$$

where x_i is the number of counts in the i -th bin, \bar{x} is the mean bin value, j and k are bin numbers for the PSTH peak (or trough) beginning and end, respectively. *FI* is positive in the case of excitation (peak) and negative in the case of inhibition (trough).

Nowadays, PSTH is often presented with its cumulative sum (CUSUM, Ellaway 1978). In this paper, we applied CUSUM only in Fig. 7, for the comparison with experimental data.

2. *Raster plot* (Fig. 2b) displays for each stimulus (test) a series of points representing the MN discharges with the same abscissa as for the PSTH, with the ordinate being the consecutive test number. In the version adopted in our program, two important modifications were introduced: (1) discharges in each test were represented by different symbols accordingly to their timing with respect to the *target interval* (i.e. the interval targeted by the synaptic volley) and (2) all tests were sorted in the order of increasing time lag between the beginning of target interval (cluster 0) and the volley arrival time (vertical broken line). Volley arrival time is calculated by adding its latency (in experiments determined from the PSTH) to the stimulus time. Note that the cluster of discharges terminating target intervals (1) consists of two fragments. The upper fragment is parallel to the cluster (0) and contains discharges terminating those intervals which were

not affected by the stimulation; they will be further called *undisturbed discharges*, as in the previous paper (Piotrkiewicz et al. 2009). The other fragment is almost vertical and contains discharges that are a response to a synaptic volley evoked by stimulation. This fragment is not always strictly vertical, especially for slow PSPs; however, it will be referred to as a “vertical cluster” for convenience. This version of the raster plot reflects changes in MN excitability within ISI, which were investigated experimentally (Kudina 1988; Kudina and Pantseva 1988; Kudina and Andreeva 2005). It has been shown that the MN does not respond to the volley if it arrives during the initial, *unexcitable* fragment of ISI and in the following *excitable* fragment the probability of response gradually increases toward the ISI end.

In one of the most recent papers (Weber et al. 2009), the authors misinterpreted the secondary maximum in the PSTH as the “period of increased excitability.” It was, however, noticed quite a while ago that not every maximum or minimum in the PSTH can be interpreted as the result of an underlying excitation or inhibition (Moore et al. 1970; Awiszus 1997; Türker et al. 1997) and that the analysis of target interval durations is necessary to properly decipher the nature of synaptic volley. This can be done in several different ways (Kudina and Pantseva 1988; Türker and Cheng 1994; Schmied and Attarian 2008). In the present study, we concentrate on the most convenient plots, with the same ordinate as those described above.

3. *Peristimulus time intervalgram* (PSTI, Fig. 2c). The abscissa of this plot is the same as for the others; the ordinate is the ISI preceding the plotted MN discharge. It provides information about the duration of those ISIs which terminate within the maxima and minima in the PSTH. To quantify the mean features of the PSTI, all intervals were sorted according to increasing peristimulus time, mean

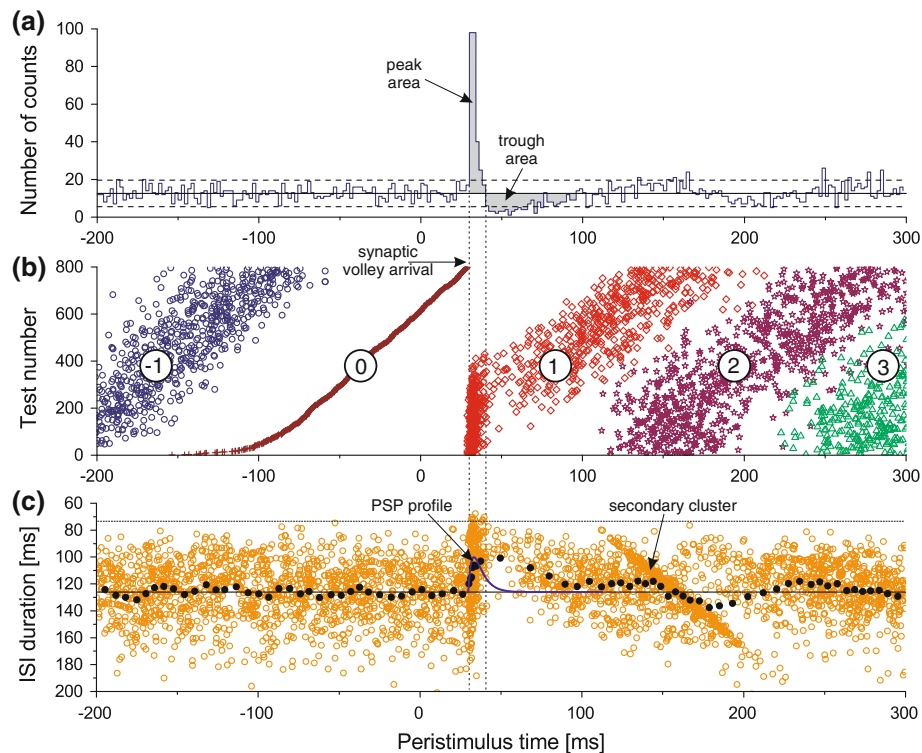


Fig. 2 Methodology of data analysis (single EPSP, parameters in Table 2): **a** PSTH; *solid horizontal line*: mean value, *broken horizontal lines*: significance limits ($\text{mean} \pm 2.5 \cdot \text{SD}$), calculated over the period of 200 ms prior to stimulus; *shaded* represent the areas of peak and trough, from which firing indexes (FIs) are calculated; **b** raster plot; -1 (*circles*): background discharges, 0 (*crosses*): discharges that begin the target intervals, 1 (*diamonds*): discharges that terminate target intervals: 2 (*asterisks*) and 3

(*triangles*): next regular discharges; **c** PSTI; *open circles*: ISIs (note that in Figs. 2, 3, 4, 5 the ordinate scale of PSTI is inverted); *black circles*: mean intervals calculated from 50 consecutive values; *solid horizontal line*: mean prestimulus ISI duration; *arrows* indicate PSP profile (its amplitude is adjusted individually for each figure) and secondary cluster, containing discharges that terminate target intervals. *Vertical dotted lines* contain the response to the EPSP. This figure was compiled from 800 tests

intervals were calculated from 50 consecutive values, overlapped by 20 (1–50, 31–80 etc.), and plotted vs. mean peristimulus time of the same 50 discharges (black points). Moreover, the average pre-stimulus ISI was calculated and shown as the solid horizontal line. In this paper, we are using the PSTI turned “upside down” for convenience of comparison with PSP profiles. In Fig. 7, we used also peristimulus time frequencygram (PSTF) compiled in the same way as the PSTI, with each ISI replaced by its reciprocal (instantaneous firing rate).

Results

To understand composite synaptic volleys, it is useful to begin from the analysis of single postsynaptic potentials (PSPs). The PSP parameters (see Table 2) underlying the results shown below were adjusted so as to conform to the FIs encountered in typical human MN responses to the just-supra-threshold electrical nerve stimulation, in particular to the stimulation of Ia afferents.

Single PSPs

Single EPSP

The simulation results obtained for a single EPSP were presented in Fig. 2. The MN responses created here a distinct peak (FI = 26.9%) in the PSTH (Fig. 2a). The peak is reflected in the vertical clusters of points in the raster plot (Fig. 2b) and in the PSTI (Fig. 2c). In the PSTI, the ISIs corresponding to this cluster exceed slightly the range of background intervals, and the mean values are shorter than the pre-stimulus average (note the inverted ordinate scale). The peak of the PSTH is followed by a long (almost 60 ms) period of decreased discharge probability (FI = -25.5%), which is not surprising given the synchronization of discharges in the response peak. Note that the FIs of peak and trough in simulated PSTH are virtually equal. The trough corresponds to the cluster of undisturbed discharges in the raster plot, and to the fragment of the PSTI where the mean ISI values are shorter than the pre-stimulus average. It is important to note that

this shortening continues beyond the duration of the EPSP used in the simulation (EPSP profile indicated by an arrow in Fig. 2c) and is associated with the decreased number of longer ISIs.

The second, diffused maximum of the PSTH (Fig. 2a) appears approximately 125 ms after the peak, which is the mean duration of background ISI. As is obvious from the raster plot, the secondary discharges (next to those synchronized in the primary peak) are mostly responsible for this maximum, thus it is an “echo” of the primary peak. It corresponds to the secondary (oblique) cluster of the PSTI, created by the discharges terminating those intervals that begin in the primary cluster.

Single IPSP

The arrival of the IPSP evokes a primary trough (FI = -10.1%) in PSTH (Fig. 3a), followed by a maximum with similar FI (11.0%). The maximum corresponds to the diffused, almost vertical cluster in the raster plot (Fig. 3b) and is associated with interval lengthening, manifested in the PSTI as the period of prolonged mean ISI values (directed downwards because of the inverted scale). Note that the

IPSP end corresponds to the maximum in the PSTH and to the center of vertical clusters in the raster plot and the PSTI. After a time equal to the mean ISI, a secondary oblique trough is visible in the PSTI (Fig. 3c), being an “echo” of the primary trough (analogous to the oblique cluster in Fig. 2c). The time course of the mean values in the PSTI is very different from the IPSP profile indicated by an arrow.

Composite volleys

EPSP + IPSP

Figure 4 presents the simulation results for an EPSP followed by an IPSP delivered 6 ms later. Here, after the PSTH peak of FI = 10.0%, the trough of FI = -15.7% appears (visible also in the raster plot and PSTI). Note that the trough has a substantially bigger area than the peak. Moreover, its area is also bigger than that of the trough created by a single IPSP (Fig. 3), despite the same IPSP parameters used in the simulation of both cases. In the PSTI, in contrast to the trials with a single EPSP and IPSP, neither interval shortenings nor elongations are visible

Fig. 3 Simulation results for the single IPSP (amplitude -2 mV): **a** PSTH; **b** raster plot; **c** PSTI; IPSP profile indicated by an arrow. Vertical broken lines mark limits of the primary trough and indicate the next maximum, corresponding to the end of IPSP. Other symbols as in Fig. 2. Figures 3, 4, 5 were compiled from 1,000 tests

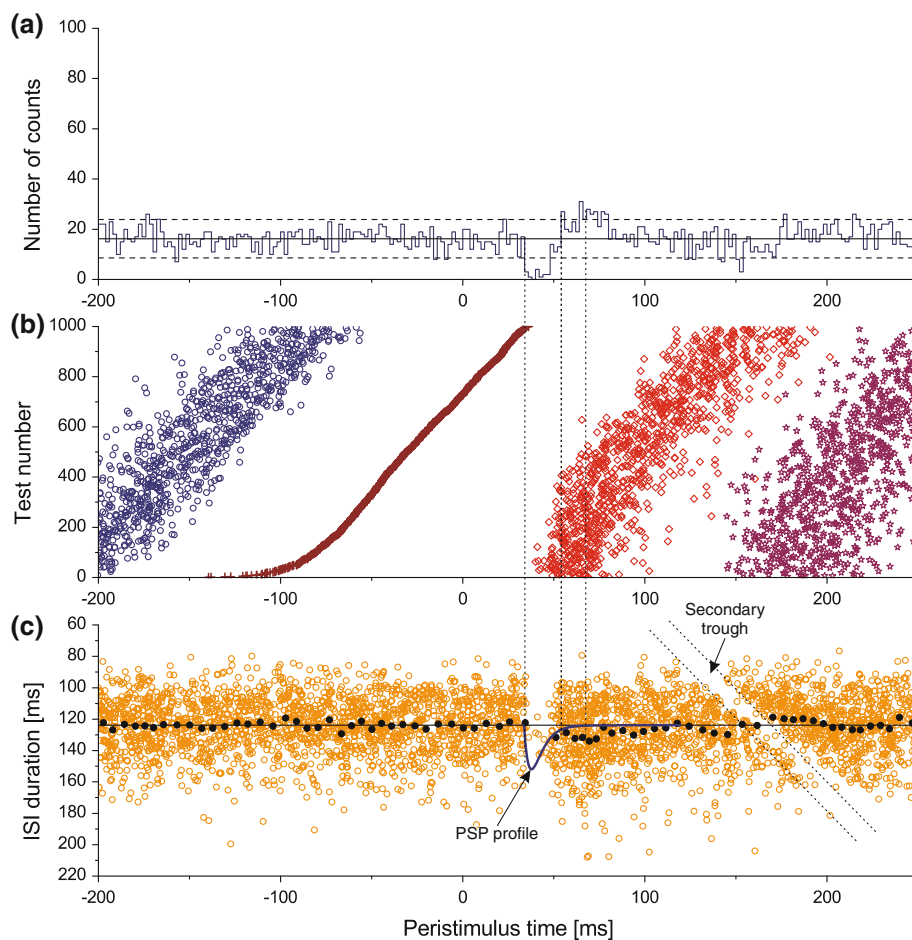
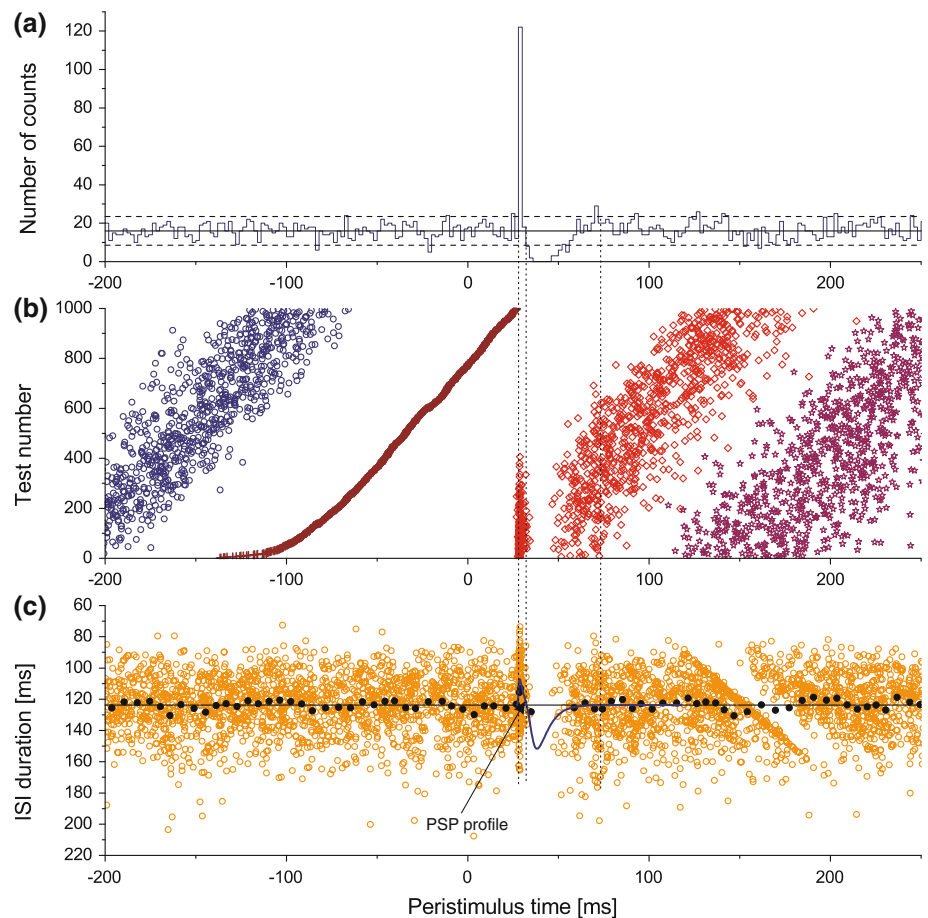


Fig. 4 Simulation results for EPSP (amplitude 1.4 mV) followed after 6 ms by IPSP (amplitude -2 mV): **a** PSTH; **b** raster plot; **c** PSTI: PSP profile indicated by an *arrow*. Vertical broken lines mark limits of the primary peak and indicate the next maximum. Other symbols as in Fig. 2



beyond the primary cluster; also the PSTH maximum after the trough is hardly visible.

If the IPSP arrives with a bigger delay, it does not affect the after-effects of the EPSP. Instead, it prolongs the intervals that were supposed to end within the secondary cluster, moving this cluster down, toward longer ISIs and longer poststimulus times (not illustrated).

IPSP + EPSP

The results for the opposite combination, an IPSP followed by an EPSP with 13 ms delay, are presented in Fig. 5. In the PSTH, the trough of $FI = -8.59\%$ and the following maximum ($FI = 12.18\%$) are visible. Note that this time the maximum has a substantially bigger area, which indicates the contribution of the extra EPSP. The raster plot presents a single vertical cluster corresponding to the maximum in the PSTH. The rising phase of the EPSP was almost completely consumed by the decaying phase of the IPSP (see the PSP profile in Fig. 5c); the remainder, however, is very steep, which gives rise to the prominent PSTH maximum. In the corresponding area in the PSTI, the distribution of ISI durations does not differ from that of the background intervals, which is illustrated by the

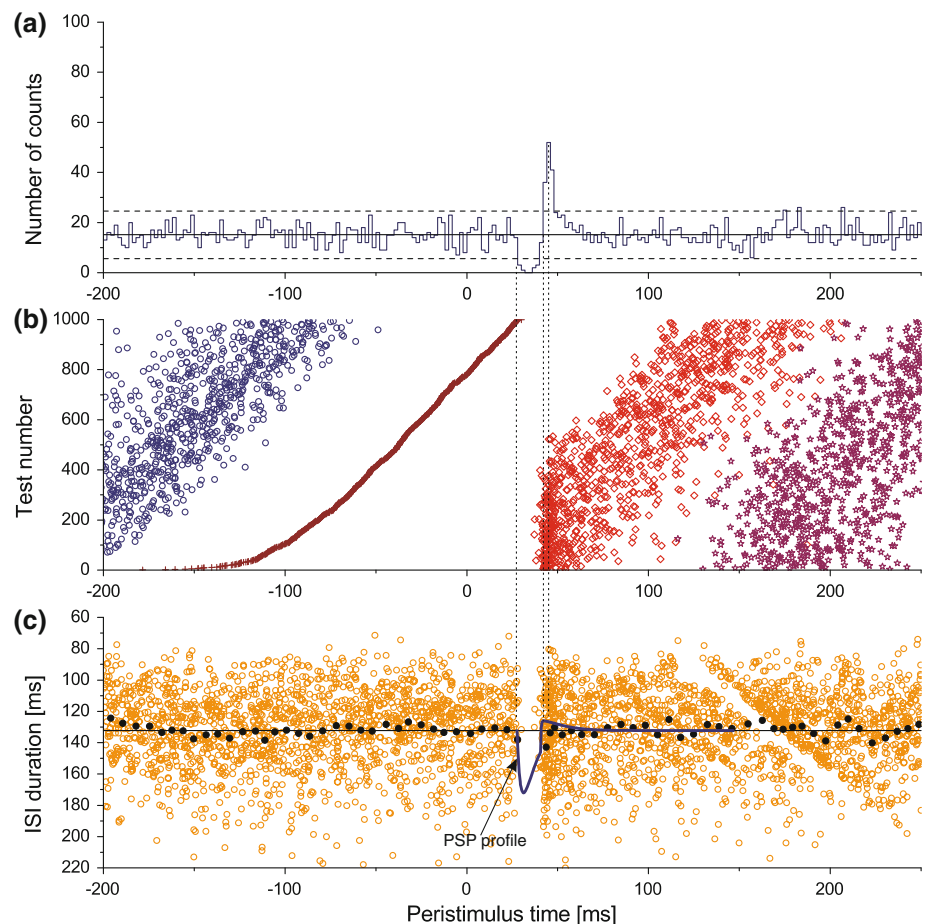
fluctuations of mean bin values around the pre-stimulus average. However, this happens only when the EPSP arrives within a short time after the IPSP. When both PSPs are separated by a longer time, their effects separate in all plots (not illustrated).

Discussion

Limitations of the model

The threshold-crossing model, used for the simulations presented in this paper, is more advanced than many other models of this type; however, it does not include all membrane mechanisms, which may influence MN excitability. The compound PSPs, which shape MN response to the stimulation analyzed by applied output measures, are in fact net potentials evoked by ‘effective synaptic current’ (Heckman and Binder 1988) transferred to the soma from multiple synapses, located mostly on dendrites. The final shape of these net potentials is influenced also by the neuromodulatory inputs (Heckman et al. 2009), which are not included in our model. However, it seems unlikely that the shapes of dendritic PSPs and the contribution of the

Fig. 5 Simulation results for IPSP (amplitude -2 mV) followed after 13 ms by EPSP (amplitude 1.4 mV): **a** PSTH; **b** raster plot; **c** PSTI: PSP profile indicated by an *arrow*. Vertical broken lines mark limits of the trough and indicate the next maximum. Other symbols as in Fig. 2



persistent inward currents could be assessed by the output measures commonly applied in human experiments and in the present study.

The spike threshold time course in the model is simplified, whereas in fact, it is also influenced by synaptic noise (Piotrkiewicz and Brette 2011). This and other phenomena, which may alter MN response to given PSP, in particular, delayed excitation (Reyes and Fetz 1993) and AHP summation (Calvin and Schwindt 1972; Ito and Oshima 1962) are not included in this model. The effect of AHP summation, however, would be significant only after large ISI shortenings, which are not dealt with in this paper.

There is no exact information on the structure of synaptic noise in real MNs, so in modeling studies, various solutions were applied. For example, Powers and Binder (2000) applied two variants of random noise with Gaussian amplitude distribution and relatively flat power spectrum up to 500 Hz or to 160 Hz, with the second variant considered to be more physiological. In our model, the synaptic noise is an integral part of the tonic synaptic inflow. The parameters of constituent PSP trains were chosen to fit the experimental dependency of standard deviation of ISIs on their mean value obtained from the

MNs supplying human brachial biceps (Fig. 2 of our previous paper Piotrkiewicz et al. 2009). This is certainly not the unique solution, so the inflow and in particular the frequency content of its noisy component may be different from that, which can be encountered in live MN. Nevertheless, a few additional simulation runs with the higher-frequency noise yielded qualitatively the same results, so it seems doubtful that the noise structure could influence the conclusions drawn from this study. However, the analysis of the impact of the structure of synaptic inflow on the model output deserves undoubtedly a separate study.

The usefulness of this model was confirmed by comparing the results of simulations with those of experiments, both animal and human. The simulated large and long-lasting EPSP made the same impact on the output measures (Piotrkiewicz et al. 2009) as that presented by Türker and Powers (1999), despite the different noise structure applied in both studies. Also simulations of human experiments applying nerve stimulation (Piotrkiewicz 2007) reproduced faithfully main results obtained by Kudina and Andreeva (2005). Thus, we have reasons to think that this model is a proper tool for analysis of stimulus-correlated changes in human MN firing characteristics.

Synchronization-related effects

A stimulus-evoked single PSP in a MN results in a time-lock of a certain number of discharges with synaptic volley, visible in all plots applied as the output measures. Figure 6 presents a schematic explanation for the synchronization evoked by the single EPSP (a) and single IPSP (b).

The differences between the impact exerted on PSTI by EPSP and IPSP go far beyond the difference in their polarities. The rising edge of the EPSP may evoke an extra discharge, which would interrupt the ISI and shorten it. Thus, the responses to EPSP would become synchronized with respect to the stimulus with the latency corresponding to the time of EPSP arrival (Fig. 6a). For a given EPSP amplitude, the most substantial shortenings are due to the volleys arriving early in the excitable fragment of ISI; toward the ISI end, the shortenings become negligible (despite the increasing MN excitability). An EPSP of small amplitude is able to evoke a response only when the membrane potential is close to the threshold, i.e., at the end of ISI, and this is why the ISI durations corresponding to the primary cluster in the experimental PSTFs obtained by just-suprathreshold stimulation often do not exceed the limits of background values (see experimental data from Prasartwuth et al. 2008 in our Fig. 7a). This explains also why the PSTI is less sensitive to very small EPSPs than the PSTH.

The arrival of a single IPSP is demonstrated by the trough in the PSTH and other plots. The target intervals

are prolonged, which decrease the mean values in the PSTI. The discharges terminating target intervals tend to be synchronized with the end of the IPSP (Fig. 6b), and this synchronization is responsible for the diffused maximum in the PSTH and corresponding clusters in the raster plot and the PSTI. Thus, the simulation results point to the possibility of roughly estimating IPSP duration from the PSTH. In contrast to the EPSP, the impact of the IPSP on the PSTI is maximal when it arrives at the end of a target interval, which is in concert with the experimental results (Kudina 1980; Kudina and Pantseva 1988). However, the discharges related to the IPSP end are strongly influenced by synaptic noise, since, the membrane potential approaches threshold very slowly. Therefore, the maximum of the PSTH and corresponding clusters in other plots are diffused. Noise is also responsible for the extended period of increases in the mean ISI duration of the PSTI (beyond the IPSP duration). The impact of noise would be even greater in the experimental work, where the MN firing rate is kept low (which means that the ISI variability is high) and the number of stimuli is limited. In these conditions, it may be impossible to determine the maximum corresponding to the IPSP end.

It has been shown in the Results section that the single short EPSP can result in the mean ISI shortening lasting much longer than EPSP itself. This shortening, corresponding to firing rate increase, is repeatedly interpreted as the influence of long-lasting excitation (e.g. Binboğa et al. 2011; Prasartwuth et al. 2008). To resolve this discrepancy,

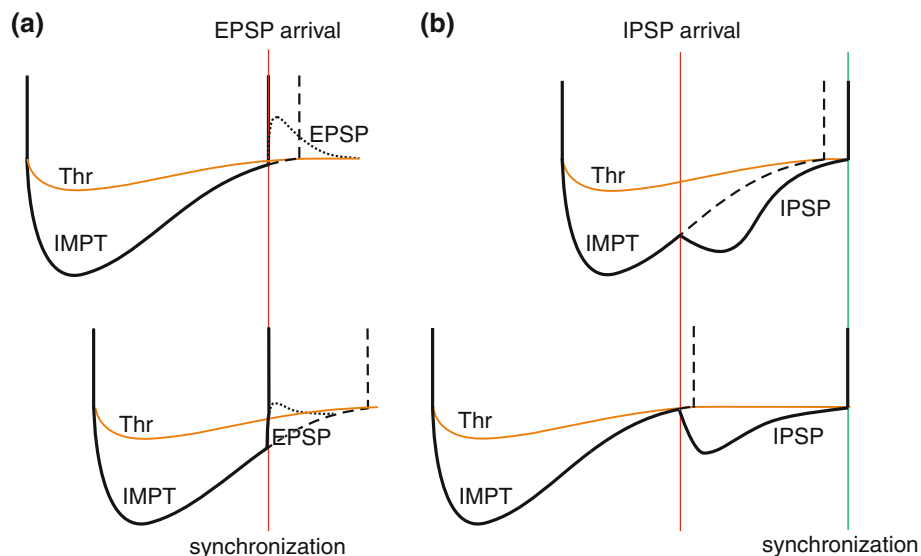
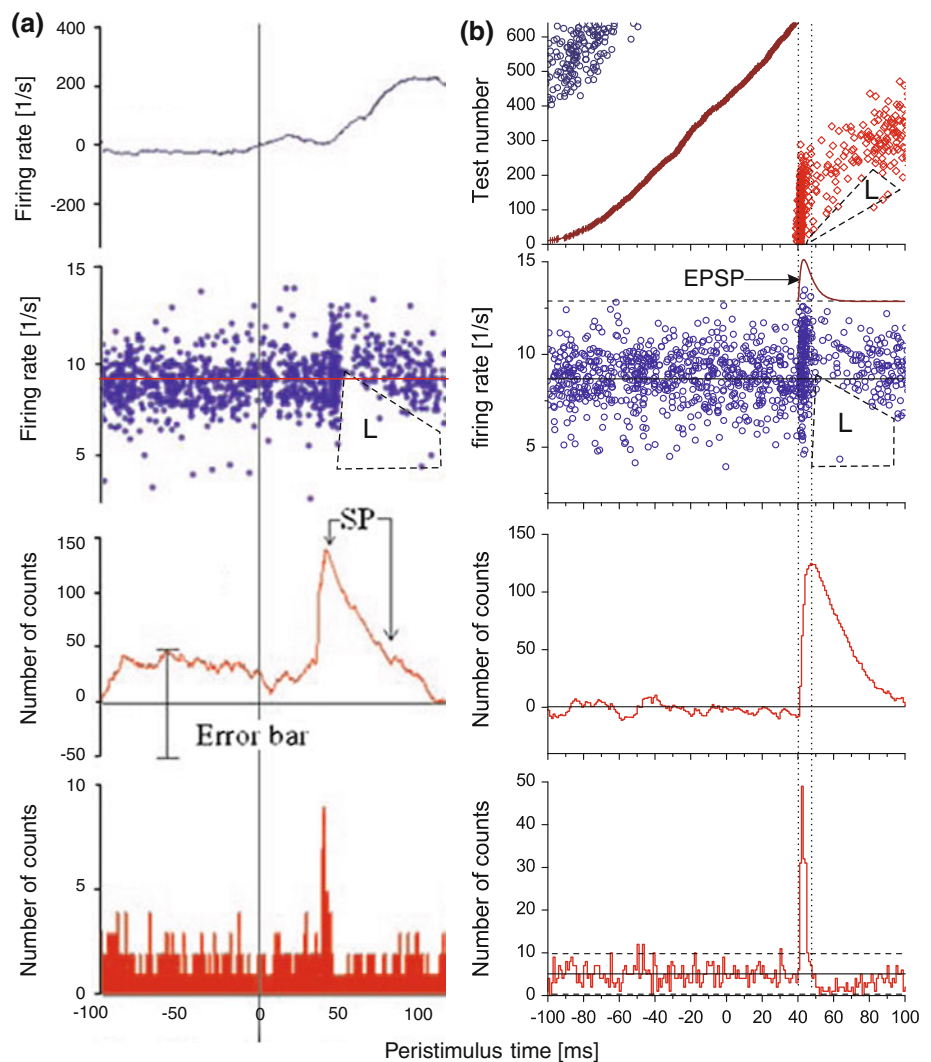


Fig. 6 Schematic representation of the interaction of single PSPs with interspike membrane potential trajectories (IMPT) of a model MN in target interval: **a** EPSP, responses synchronized with EPSP arrival; **b** IPSP, discharges terminating prolonged ISIs synchronized with IPSP end. For each type of stimulation, only two cases are shown, with little change (*upper panels*) and big change (*lower*

panels) in the ISI duration. Thr, threshold; the *lines* above the threshold, schematic representation of MN spikes; broken IMPT fragments and spikes show what would have happened if the MN had not responded to the synaptic volley; *dotted* profiles, EPSP fragments extinguished due to spike generation

Fig. 7 Comparison of PSTFs from the experiment and computer simulation: **a** the experimental results showing ‘Ia-only’ response of a tibialis anterior MU to nerve stimulation (adapted from Fig. 2 of Prasartwuth et al. 2008, with kind permission of the author and Springer Science+Business Media); **b** simulation results (EPSP with latency 41 ms; time parameters given in Table 2). The panels from bottom to top: PSTH, PSTH CUSUM, PSTF; uppermost panels: **a** PSTF CUSUM, **b** raster plot. In **a**, SP, silent period; in PSTFs (**a**, **b**) and raster plot (**b**) indicated are areas (L) with limited number of longer ISIs; in **b** dotted vertical lines indicate response range



we performed simulations aimed toward the reproduction of the ‘H-reflex only’ results obtained from the tibialis anterior muscle by the stimulation of the peroneal nerve (Prasartwuth et al. 2008, their Fig. 2). Figure 7 presents the comparison of experimental results (a) with the results of simulation with a single EPSP of amplitude 1.7 mV and duration 31.6 ms (b). The presentation of both experimental and simulation results is limited to the most relevant fragment of peristimulus time, from -100 to 100 ms.

It can be noticed that the fragment of peristimulus time marked SP in Fig. 7a corresponds in PSTF to the area with markedly decreased number of points (‘L’ area). Such areas can also be seen in the simulated PSTF and raster plot. It is important to note that the discharges missing from this areas correspond to the longest intervals. Moreover, it may be deduced from the raster plot that missing intervals are those, to which EPSP arrived at their terminal, most effective fragment (cf. Kudina 1988; Kudina and Andreeva 2005), so they responded to the EPSP, and their

terminating discharges ended in the synchronization cluster.

Thus, the elevation of firing rates following the direct response to the EPSP can be reliably explained as the synchronization-related effect of a single short EPSP. The question arises, whether this is the only explanation for the effect in the real data, or whether the prolonged decaying phase of longer EPSP could also participate in this effect.

For the first, the short EPSP is more compatible to the Ia afferent EPSPs, whose durations were estimated in human by Ashby and Labelle (1977) and Sabbahi and Sedgwick (1987) by double-pulse stimulation. The durations were comprised in the range 5–20 ms (Ashby and Labelle 1977) and 2–12 ms (Sabbahi and Sedgwick 1987).

For the second, the fact that in rat brain stem slice experiments huge and long EPSPs evoked responses on their decaying phases (Türker and Powers 1999) cannot justify the same explanation for the results of human experiments, where just-suprathreshold stimulation was

applied. We have shown in our previous paper (Piotrkiewicz et al. 2009) that the EPSP similar to those applied in (Türker and Powers 1999) can indeed evoke a response during considerable part of its decaying phase, which is indicated by the elevation of firing rates in PSF beyond the limits of prestimulus rates, lasting longer than the peak in PSTH. However, in fact, the discharges corresponding to the terminal fragment of PSF were mixed with the secondary discharges. This was clearly visible at low firing rates (cf. Fig. 7b in Piotrkiewicz et al. 2009), when the terminal PSF fragment clearly separated from the response. If the pre-stimulus firing rate was properly adjusted to the duration of EPSP (cf. Fig. 7a in Piotrkiewicz et al. 2009), the secondary discharges merged with the response and the result created the illusion that the PSF reproduced the whole EPSP shape. The response in Fig. 7a of the present paper and in other experimental PSFs presented in (Binboğa et al. 2011; Prasartwuth et al. 2008) is limited to the duration of PSTH peak and often does not exceed pre-stimulus rates; thus, the decaying phase of the EPSP may be responsible for the extra discharges only during its short initial fragment (see PSP profile in Fig. 7b).

Finally, the assumption that in human studies the dispersion of times of Ia EPSP arrival to a MN is much larger than in animal experiments (Türker et al. 1997) may be justified in case of the tendon tap; however, during just-suprathreshold electrical stimulation, only few Ia fibers of lowest threshold are excited, so the large dispersion cannot be expected. This issue was investigated by Burke et al. (1984) who determined the rise time of EPSPs evoked in single MNs by tendon percussion at 7.5 ± 2.3 ms, but of those evoked by electrical stimulation at 2.4 ± 1.4 ms; the latter values are compatible with those estimated by Ashby and Labelle (1977).

The presence of this synchronization-related effect is quite fortunate, since it allows us to distinguish the pattern created by a single EPSP from those related to the more complex PSPs (e.g. EPSP + IPSP); nevertheless, it is not the evidence of a long-lasting net excitation.

Guidelines for decoding the stimulus-correlated MN firing patterns

The results presented above were obtained from computer simulations, where the number of stimuli delivered may be as high as needed and the level of MN excitation is constant. In experimental practice, the number of stimuli is limited, and the results often contain a mixture of different firing rates, so the resulting plots may be less clear than those presented in this paper. Nevertheless, we were able to decode the composition of the experimental synaptic volley and produce patterns reproducing the experimental results quite well. This allows us to hope that the guidelines for

decoding the stimulus-correlated MN firing, presented below, will be helpful with the interpretation of experimental results.

Qualitative decoding

The typical manifestation of a single EPSP is a peak in the PSTH, corresponding to the vertical clusters in the raster plot and the PSTI. They are followed by synchronization-related effects: the trough in the PSTH (of FI approximately equal to that of the peak) and corresponding area in the PSTI where mean values are shorter due to the missing longer intervals. It is important to determine the fragment of peristimulus time, related to the response to excitation. It is limited to the post-stimulus time range, during which the PSTI values are shorter than the shortest pre-stimulus ISI, and/or the number of counts within PSTH peak significantly exceeds mean value. The secondary features are the diffused maximum in the PSTH and the oblique cluster in the PSTI, both delayed by a time approximately equal to the mean ISI duration and related to the cluster of secondary discharges in the raster plot.

A single IPSP is manifested in the PSTH by the trough and following maximum, for which the discharges related to the IPSP end, and diffused by noise, are responsible. The maximum corresponds to the diffused clusters in the raster plot and PSTI; the mean interval values of PSTI cluster are longer than the pre-stimulus average. After a time approximately equal to the mean ISI duration, the secondary trough may be visible in the PSTH and PSTI if the primary trough was big enough.

In composite PSPs, any component is manifested as a separate cluster in the raster plot and PSTI, except for the cases when the IPSP is immediately followed by an EPSP. When the components follow each other with considerable delays, the features characteristic for the single EPSPs or IPSPs are easy to distinguish. When PSPs of opposite signs follow each other with only a few milliseconds delay, their synchronization-related effects in the PSTI cancel each other. Therefore, if the ISI duration is not increased after the PSTH trough or not decreased after the PSTH peak, it indicates the coincidence of EPSP and IPSP.

Quantitative decoding

The most convenient estimate of EPSP amplitude is FI, which may be calculated from the PSTH data; for IPSP, however, it can be applied only when the count number in the trough is higher than zero. Although quantification of changes in instantaneous firing rate provides a better measure of EPSP amplitude than FI (Piotrkiewicz et al. 2009; Powers and Türker 2010b), it is limited to EPSPs of amplitudes higher than 1 mV (Türker and Powers 1999),

whereas FI is derived from PSTH, which is more sensitive to PSPs of small amplitudes. The quantitative estimation of a PSP amplitude, which would be scaled in mV, is impossible, since the results are influenced by many factors other than PSP amplitude (Gustafsson and McCrea 1984; Piotrkiewicz et al. 2009; Powers and Türker 2010b), such as the amount of synaptic noise or AHP duration, which are either not measurable in human experiments or their estimation is difficult and requires too many assumptions to be accurate. For the EPSP, only the duration of its rising phase may be roughly estimated, although it should be kept in mind that the estimate is influenced by noise and thus is always longer than the real value. The estimation of EPSP duration is impossible, at least in case of electrical stimulation with low intensity, where only its initial fragment influences MN firing. The terminal fragment of EPSP is lost and thus cannot have any effect on the output measures (Piotrkiewicz et al. 2009). For the IPSP, the estimation of total duration may be possible. As indicated above, this can be done only from the PSTH: IPSP onset is indicated by the beginning of the trough, and its end by the post-trough maximum. However, when the MN firing rate is low (which is associated with high ISI variability) and the number of stimuli is not sufficient, the maximum on PSTH may be difficult to determine.

Conclusions

The results of this study provide directions for the proper interpretation of the experimental results of stimulus-related MN firing in terms of synaptic volleys evoked by the stimulation, including results obtained with transcranial magnetic stimulation (Todd et al. 2011). The essential output measures allowing for qualitative decoding are PSTH, raster plot and PSTI or PSTF. Both PSTF and PSTI are very convenient for analysis of stimulus-evoked changes in ISI duration, which is often necessary to determine the sign of the underlying synaptic volleys. However, as has been shown above, even PSTI and PSTF are not free from synchronization-evoked effects, which should be taken into account. The raster plot may also be very useful, since in contrast to the previously used versions, it allows distinguishing MN discharges that are responsible for a given PSTH or PSTI/PSTF pattern and provides information on the change of MN excitability within ISI.

Türker and Powers in their extensive studies (Türker and Powers 1999, 2002, 2003, 2005; Powers and Türker 2010a) have proven that not every maximum in the PSTH can be interpreted as an excitation, nor minimum, as an inhibition. The simulation results presented above show that not every firing rate increase in a PSTF can be interpreted as a net excitation, and that even no change in mean firing rate

bears information about the presence of the coincidence of inhibition and excitation, whose effects cancel each other.

Acknowledgments The authors are indebted to the anonymous reviewers, whose valuable criticism greatly contributed to the final shape of this paper. Special thanks are due to Prof. Kemal Türker for kind permission to use his figure and for fiery discussions, which provided the arguments for the explanation of synchronization-related effects. This research was supported by statutory grants for IBBE and IITP. The mutual contacts between the authors were possible due to the agreement between Polish and Russian Academies of Sciences.

Open Access This article is distributed under the terms of the Creative Commons Attribution Noncommercial License which permits any noncommercial use, distribution, and reproduction in any medium, provided the original author(s) and source are credited.

References

- Ashby P, Labelle K (1977) Effects of extensor and flexor group I afferent volleys on the excitability of individual soleus motoneurons in man. *J Neurol Neurosurg Psychiatr* 40:910–919
- Ashby P, Zilm D (1982a) Characteristics of postsynaptic potentials produced in single human motoneurons by homonymous group I volleys. *Exp Brain Res* 47:41–48
- Ashby P, Zilm D (1982b) Relationship between EPSP shape and cross-correlation profile explored by computer simulation for studies on human motoneurons. *Exp Brain Res* 47:33–40
- Awiszus F (1988) Continuous functions determined by spike trains of a neuron subject to stimulation. *Biol Cybern* 58:321–327
- Awiszus F (1997) Spike train analysis. *J Neurosci Meth* 74:155–166
- Binboğa E, Prasartwuth O, Pehlivan M, Türker K (2011) Responses of human soleus motor units to low-threshold stimulation of the tibial nerve. *Exp Brain Res* 213:73–86
- Burke RE (1967) Composite nature of the monosynaptic excitatory postsynaptic potential. *J Neurophysiol* 30:1114–1137
- Burke D, Gandevia SC, McKeon B (1984) Monosynaptic and oligosynaptic contributions to human ankle jerk and H-reflex. *J Neurophysiol* 52:435–448
- Button DC, Gardiner K, Marqueste T, Gardiner P (2006) Frequency-current relationships of rat hindlimb α -motoneurons. *J Physiol Lond* 573:663–677
- Calvin WH (1974) Three modes of repetitive firing and the role of threshold time course between spikes. *Brain Res* 69:341–346
- Calvin WH, Schwindt PC (1972) Steps in production of motoneuron spikes during rhythmic firing. *J Neurophysiol* 35:297–310
- Coombs J, Eccles J, Fatt P (1955) Excitatory synaptic action in motoneurons. *J Physiol Lond* 130:374–395
- Curtis D, Eccles CJ (1959) The time courses of excitatory and inhibitory synaptic actions. *J Physiol Lond* 145:529–546
- Ellaway PH (1978) Cumulative sum technique and its application to the analysis of peristimulus time histograms. *Electroencephalogr Clin Neurophysiol* 45:302–304
- Gorassini MA, Norton JA, Nevett-Ducherer J, Roy FD, Yang JF (2009) Changes in locomotor muscle activity after treadmill training in subjects with incomplete spinal cord injury. *J Neurophysiol* 101:969–979
- Guertin PA, Hounsgaard J (1999) Non-volatile general anaesthetics reduce spinal activity by suppressing plateau potentials. *Neuroscience* 88:353–358
- Gustafsson B, McCrea D (1984) Influence of stretch-evoked synaptic potentials on firing probability of cat spinal motoneurons. *J Physiol Lond* 347:431–451

- Heckman C, Binder MD (1988) Analysis of effective synaptic currents generated by homonymus Ia afferent fibres in motoneurons in the cat. *J Neurophysiol* 60:1946–1966
- Heckman CJ, Johnson M, Mottram C, Schuster J (2008) Persistent inward currents in spinal motoneurons and their influence on human motoneuron firing patterns. *Neuroscientist* 14:264–275
- Heckman CJ, Mottram C, Quinlan K, Theiss R, Schuster J (2009) Motoneuron excitability: the importance of neuromodulatory inputs. *Clin Neurophysiol* 120:2040–2054
- Ito M, Oshima T (1962) Temporal summation of after-hyperpolarization following a motoneurone spike. *Nature* 195:910–911
- Jakubiec M, Piotrkiewicz M (2004) Computer system for analysis of recurrent inhibition between human motoneurons. *Biocyber Biomed Eng* 24:3–14
- Kudina LP (1980) Reflex effects of muscle afferents on antagonist studied on single firing motor units in man. *Electroencephalogr Clin Neurophysiol* 50:214–221
- Kudina LP (1988) Excitability of firing motoneurons tested by Ia afferent volleys in human triceps surae. *Electroencephalogr Clin Neurophysiol* 69:576–580
- Kudina L, Andreeva R (2005) Discharge frequency and excitability of human firing motoneuron. *Biophysics* 50:778–783
- Kudina LP, Pantseva RE (1988) Recurrent inhibition of firing motoneurons in man. *Electroencephalogr Clin Neurophysiol* 69:179–185
- Miles TS, Türker KS, Le TH (1989) Ia reflexes and EPSPs in human soleus motor neurones. *Exp Brain Res* 77:628–636
- Moore GP, Segundo JP, Perkel DH, Levitan H (1970) Statistical signs of synaptic interaction in neurons. *Biophys J* 10:876–900
- Piotrkiewicz M (1999) An influence of afterhyperpolarization on the pattern of motoneuronal rhythmic activity. *J Physiol Paris* 93:125–133
- Piotrkiewicz M (2007) Analysis of factors underlying excitability of human motoneurons by means of computer simulations [in Polish]. XV Conference of Biocybernetics and Biomedical Engineering, Wrocław
- Piotrkiewicz M, Kudina L, Hausmanowa-Petrusewicz I, Zhoukovskaya N, Mierzejewska J (2001) Discharge properties and afterhyperpolarization of human motoneurons. *Biocyber Biomed Eng* 21:53–75
- Piotrkiewicz M, Kudina L, Mierzejewska J (2004) Recurrent inhibition of human firing motoneurons (experimental and modelling study). *Biol Cybern* 91:243–257
- Piotrkiewicz M, Kudina L, Jakubiec M (2009) Computer simulation study of the relationship between the profile of excitatory postsynaptic potential and stimulus-correlated motoneuron firing. *Biol Cybern* 100:215–230
- Platkiewicz J, Brette R (2011) Impact of fast sodium channel inactivation on spike threshold dynamics and synaptic integration. *PLoS Comput Biol* 7:e1001129
- Powers RK, Binder MD (1996) Experimental evaluation of input-output models of motoneuron discharge. *J Neurophysiol* 75:367–379
- Powers RK, Binder MD (2000) Relationship between the time course of the afterhyperpolarization and discharge variability in cat spinal motoneurons. *J Physiol Lond* 528:131–150
- Powers RK, Türker KS (2010a) Deciphering the contribution of intrinsic and synaptic currents to the effects of transient synaptic inputs on human motor unit discharge. *Clin Neurophysiol* 121:1643–1654
- Powers RK, Türker KS (2010b) Estimates of EPSP amplitude based on changes in motoneuron discharge rate and probability. *Exp Brain Res* 206:427–440
- Prasartwuth O, Binboga E, Türker KS (2008) A study of synaptic connection between low threshold afferent fibres in common peroneal nerve and motoneurons in human tibialis anterior. *Exp Brain Res* 191:465–472
- Reyes AD, Fetzer EE (1993) Two modes of interspike interval shortening by brief transient depolarizations in cat neocortical neurons. *J Neurophysiol* 69:1661–1672
- Sabbahi MA, Sedgwick EM (1987) Recovery profile of single motoneurons after electrical stimuli in man. *Brain Res* 423:125–134
- Schmied A, Attarian S (2008) Enhancement of single motor unit inhibitory responses to transcranial magnetic stimulation in amyotrophic lateral sclerosis. *Exp Brain Res* 189:229–242
- Todd G, Rogash NC, Türker KS (2011) Transcranial magnetic stimulation and peristimulus frequencygram. *Clin Neurophysiol*, doi:10.1016/j.clinph.2011.09.019
- Türker KS, Cheng HB (1994) Motor-unit firing frequency can be used for the estimation of synaptic potentials in human motoneurons. *J Neurosci Meth* 53:225–234
- Türker KS, Powers RK (1999) Effects of large excitatory and inhibitory inputs on motoneuron discharge rate and probability. *J Neurophysiol* 82:829–840
- Türker KS, Powers RK (2002) The effects of common input characteristics and discharge rate on synchronization in rat hypoglossal motoneurons. *J Physiol* 541:245–260
- Türker KS, Powers RK (2003) Estimation of postsynaptic potentials in rat hypoglossal motoneurons: insights for human work. *J Physiol Lond* 551:419–431
- Türker KS, Powers RK (2005) Black box revisited: a technique for estimating postsynaptic potentials in neurons. *Trends Neurosci* 28:379–386
- Türker KS, Yang J, Scutter SD (1997) Tendon tap induces a single long-lasting excitatory reflex in the motoneurons of human soleus muscle. *Exp Brain Res* 115:169–173
- Weber M, Ferreira V, Eisen A (2009) Determinants of double discharges in amyotrophic lateral sclerosis and Kennedy disease. *Clin Neurophysiol* 120:1971–1977
- Windels F, Kiyatkin EA (2006) General anesthesia as a factor affecting impulse activity and neuronal responses to putative neurotransmitters. *Brain Res* 1086:104–116